Applied Catalysis B: Environmental 327 (2023) 122373

Contents lists available at ScienceDirect

Applied Catalysis B: Environmental

journal homepage: www.elsevier.com/locate/apcatb

Efficient electrocatalytic H_2O_2 evolution utilizing electron-conducting molecular wires spatially separated by rotaxane encapsulation

Sheng-Ying Chou [a], Hiroshi Masai [a,*], Masaya Otani [a], Hiromichi V. Miyagishi [a], Gentaro Sakamoto [b], Yusuke Yamada [b,c,**], Yusuke Kinoshita [d], Hitoshi Tamiaki [d], Takayoshi Katase [e], Hiromichi Ohta [e], Tomoki Kondo [f], Akinobu Nakada [f], Ryu Abe [f], Takahisa Tanaka [g], Ken Uchida [g], Jun Terao [a,*]

[a] Department of Basic Science, Graduate School of Arts and Sciences, The University of Tokyo, Meguro-ku, Tokyo 153-8902, Japan
[b] Department of Chemistry and Bioengineering, Graduate School of Engineering, Osaka Metropolitan University, Sugimoto, Sumiyoshi, Osaka 558-8585, Japan
[c] Research Center of Artificial Photosynthesis (ReCAP), Osaka Metropolitan University, Sugimoto, Sumiyoshi, Osaka 558-8585, Japan
[d] Department of Applied Chemistry, Graduate School of Life Sciences, Ritsumeikan University, Kusatsu 525-8577, Japan
[e] Research Institute for Electronic Science, Hokkaido University, N20W10, Kita, Sapporo 001-0020, Japan
[f] Department of Energy and Hydrocarbon Chemistry, Graduate School of Engineering, Kyoto University, Nishikyo-ku, Kyoto 615-8510, Japan
[g] Department of Materials Engineering, The University of Tokyo, Bunkyo-ku, Tokyo 113-8656, Japan

ARTICLE INFO

Keywords:
Organic-inorganic hybrid interface
Interfacial charge transfer
Cyclodextrin
Energy carrier

ABSTRACT

Immobilization of a catalytically active metal complex onto an electrode surface in highly dispersed form is crucial to assure high catalytic activity observed in solution. In this report, mononuclear Co^{II} chlorin complexes were successfully immobilized on a conductive metal-oxide electrode by using electron conducting molecular wires comprising phenylene–ethynylene-based π-conjugation covered by a linked permethylated α-cyclodextrin to enhance electrocatalysis for selective two electron reduction of molecular oxygen to hydrogen peroxide. First, the rotaxane-encapsulation effect of the molecular wire on electron transfer was examined by the comparison of electrochemical behaviors of ferrocene (Fc) molecules immobilized on an ITO substrate using the molecular wires with or without rotaxane encapsulation. Then, electrodes were modified with metalloporphyrinoids, i.e., Rh^{III}(OEP)Cl (OEP = 2,3,7,8,12,13,17,18-octaethylporphyrin) and Co^{II} chlorin through coordination with the molecular wires with pyridine moieties at the end. The electrocatalytic O_2 reduction was performed with Co^{II} chlorin immobilized on an electron-conductive metal-oxide substrate by molecular wires. The turnover frequency for H_2O_2 production using the Co^{II} chlorin coordinated by molecular wires with rotaxane encapsulation was 331 ± 75, which is significantly higher than that of 82 ± 8 obtained for Co^{II} chlorin immobilized by that without rotaxane encapsulation. These results clearly indicate that the molecular wires with rotaxane encapsulation are beneficial for Co^{II} chlorin complexes to exhibit high electrocatalytic activity and selectivity to H_2O_2.

1. Introduction

Construction of efficient energy conversion systems is critical to realize sustainable society. Especially, conversion of electrical energies generated by utilizing natural energies such as solar energy, wind energy, etc to chemical energy is important for load leveling [1]. Electrochemical generation of high energy compounds can be often catalyzed by metal complexes [2]. Hydrogen peroxide (H_2O_2) has been attracted much attention, because hydrogen peroxide can be easily produced by O_2 abundant in air with relatively low energy [3]. Some metal complexes acting as highly efficient catalysts in solution have been reported to exhibit only low activity and selectivity by immobilization onto electrode surfaces. For example, Co chlorin complex showed high catalytic activity for selective reduction of O_2 to H_2O_2 in solution, however, the selectivity to H_2O_2 decreases by loading on an electrode with conventional method because of aggregate formation [4–6].

* Corresponding authors.
** Corresponding author at: Department of Chemistry and Bioengineering, Graduate School of Engineering, Osaka Metropolitan University, Sugimoto, Sumiyoshi, Osaka 558-8585, Japan.
E-mail addresses: cmasai.h@g.ecc.u-tokyo.ac.jp (H. Masai), ymd@omu.ac.jp (Y. Yamada), cterao@g.ecc.u-tokyo.ac.jp (J. Terao).

https://doi.org/10.1016/j.apcatb.2023.122373
Received 28 October 2022; Received in revised form 30 December 2022; Accepted 3 January 2023
Available online 9 January 2023

Immobilization of metal complexes in monomeric form is demanded to exhibit their intrinsic high catalytic activity and selectivity on electrode surface as well as in solution.

Several methods have been reported to immobilize metal complexes onto electrodes surfaces [7,8]. The most widely used method is the polymer film coating where metal complexes are mounted on the electrode surface together with a polymer film to avoid leaching of the metal complexes. Metal complexes could easily aggregate on the electrode surfaces with this method, resulting the loss of catalytic activity. The covalent bonding method using chemical agents such as organosilanes guarantees monolayer formation of the metal complexes on the electrode surfaces [7], however, ligand modification is usually time consuming. Another method suitable for mononuclear structure formation is chemisorption of metal complexes onto electrode surfaces [7], however, this method can be applicable only when metal complexes strongly interact with electrode surfaces. Thus, emergence of a universal method to connect a wide variety of metal complexes onto electrode surfaces has been demanded.

Utilization of a scaffold with rigid molecular wires which can strongly connect a metal complex with an electrode seems to be a promising method for the metal complex to maintain mononuclear form. In particular, π-conjugated molecules, which possess high electrical conductivity, have been utilized for diverse organic–inorganic hybrid devices such as memory devices, solar cells, artificial photosynthesis systems and biosensors [9–11]. Specifically in the case of electrical devices including electrocatalysis, the high molecular modification density and high charge-transfer efficiency at the interface, which are governed by the morphology of the surface organic components, are critical to the device performance [12]. However, a drawback of π-conjugated molecules is formation of objectionable aggregation on surfaces owing to their strong π–π interaction (Fig. 1a) [13]. Paving the optimum conductive pathways at the interface by inhibiting π-aggregation is therefore critical to improve the electrocatalytic performance. Recently, host–guest supramolecular structures have gained importance as a promising method to inhibit π–π interaction [14–16]. The host molecules efficiently covering the π-conjugated guests inhibit unfavorable π-aggregation on electrode surfaces, where the π-conjugated guests are "insulated" by the protective host molecules from the external environment [17–19]. In particular, pseudorotaxanes, in which cyclic and axis molecules dynamically form threading structures [20], have been utilized for hybrid modification because of their facileness in situ preparation [21]. However, owing to their lack of stoppers, pseudorotaxanes can dynamically dissociate to form irregular structures on the hybrid interfaces, including aggregated π-conjugated molecules and empty cyclic molecules. To address these concerns, we introduced the [1]rotaxane strategy (Fig. 1 b and c) [22,23]. In contrast to common rotaxane structures, [1]rotaxane structures prevent macrocycles from dissociating, without any bulky stopper units in the rotaxanes.

In this study, we synthesized an insulated π-conjugated molecule as an electron conductive molecular wire to achieve independent immobilization on electrode surfaces. The molecular wire comprises phenylene–ethynylene (PE)-based π-conjugation, covered by a linked permethylated α-cyclodextrin (PM α–CD) as the shielding unit, and displays high solubility in organic solvents together with a deep cavity (Fig. 1c). As an anchoring moiety to the substrates, phosphonic acid was directly introduced at the end of the conjugated section, to allow strong interaction and transfer the charge to various metal oxide substrates [24] such as indium tin oxide (ITO) and fluorine-doped tin oxide (FTO), which are utilized as electrodes in electrical devices. The insulation effects were investigated to clarify the high-degree independency and excellent electrical and catalytic properties on the hybrid interface, compared to those on the uninsulated counterparts, owing to the inhibition of intermolecular interaction by encapsulation.

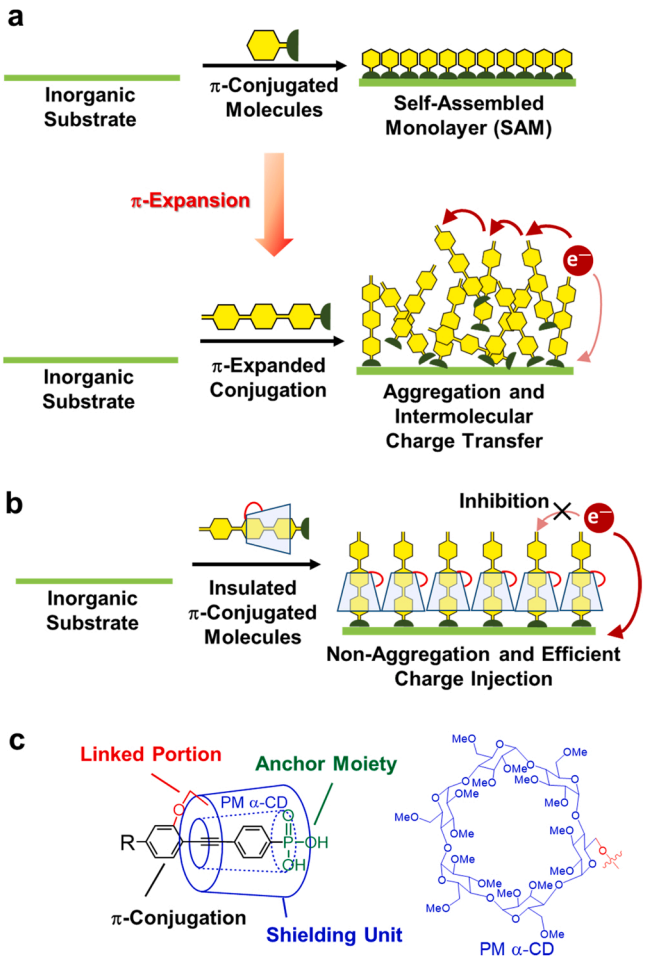

Fig. 1. (a) Conceptual illustrations of (a) SAMs constructed by unexpanded π-conjugated molecules (top) and intermolecular charge transfer caused by undesirable aggregation due to strong aromatic interaction derived from the expansion of the π-conjugated backbone (bottom). (b) Non-aggregation and efficient charge injection because of π–π interaction and intermolecular charge-transfer inhibition using the [1]rotaxane structure. (c) Molecular design of the conjugated [1]rotaxane for surface immobilization.

2. Experimental section

Solvents used for electrochemical analyses are spectroscopic grade and used as received from chemical companies. Synthesis of molecular wires, **1**–**7**, **3'**–**5'** and **S12**, are described in supporting information in detail. The molecular structure of each molecular wire is depicted in Figs. 2–5 (vide infra).

2.1. Electrode preparation

2.1.1. ITO substrates

ITO substrates (surface roughness: average 0.7 nm) for electrochemical experiments were obtained from KURAMOTO, Japan. Single crystalline ITO substrates (atomically flat terraces and steps (<0.2 nm)) for atomic force microscopy (AFM) measurements were prepared by the previously reported method [25]. The ITO substrates were annealed with ozone at 200 °C for 15 min before use.

2.1.2. Preparation of Rh^{III}(OEP)Cl–X/ ITO (X = 5 or 5')

An annealed ITO substrate was immersed in a solution of **5** or **5'** in methanol (1.0 mM) overnight at room temperature, followed by rinsing in methanol (three times) as well as chloroform (three times) and drying under nitrogen flow. Subsequently, the substrates were submerged in a

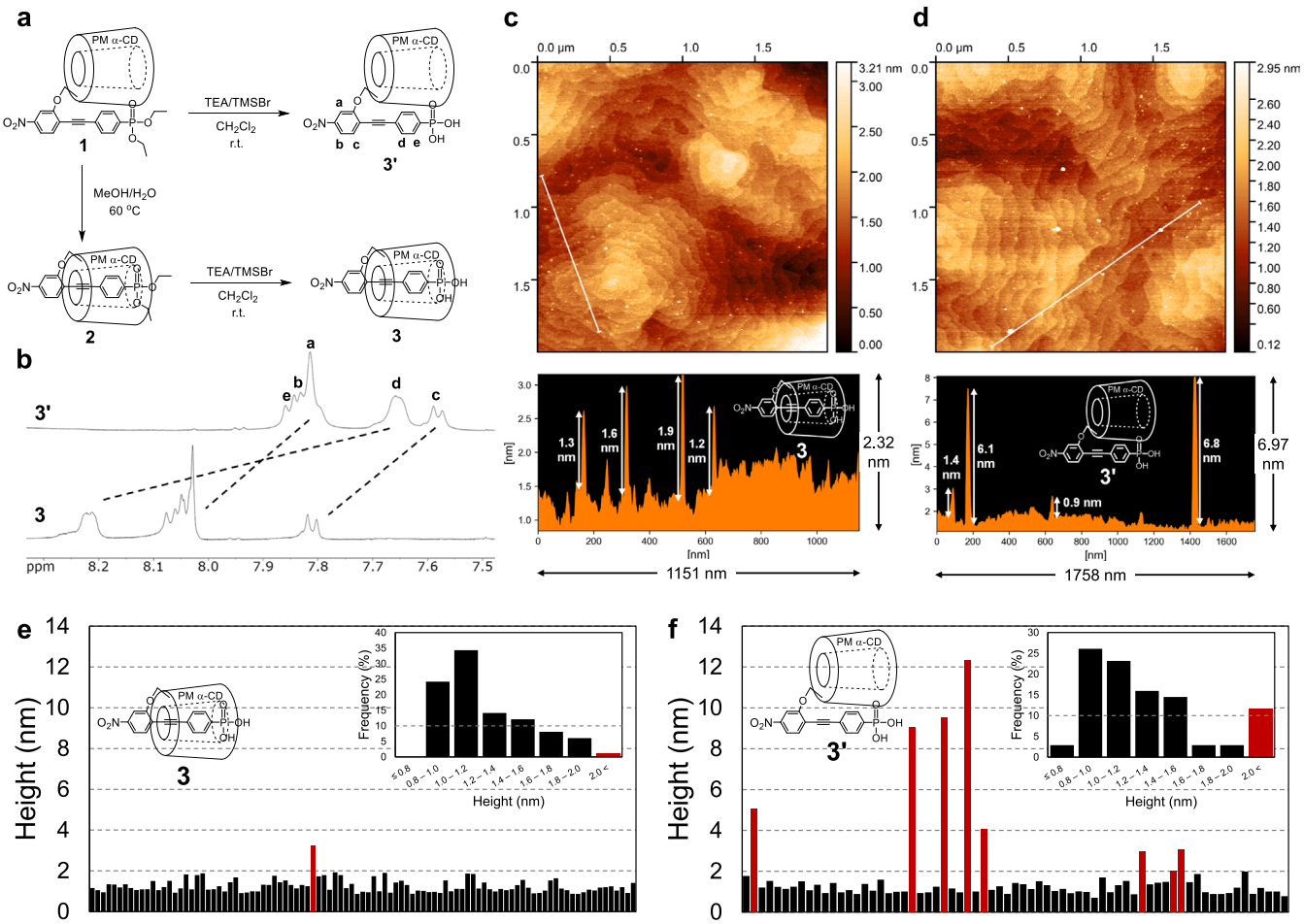

Fig. 2. (a) Synthetic route of **3** and **3'**. (b) Aromatic region in the ^{1}H NMR (500 MHz, $CDCl_3$) spectra of (top) **3'** and (bottom) **3**. AFM images of the single-crystalline ITO substrates modified by (c) **3** and (d) **3'** with the plan views and representative cross-sectional profiles (white line). Height of each protrusion of (e) immobilized **3** (99 counts) and (f) immobilized **3'** (69 counts) in the AFM image (inset: histogram of height analyses).

solution of **Rh^{III}(OEP)Cl** in CH_2Cl_2 (200 μM) for 2 h, followed by rinsing in CH_2Cl_2 (three times) as well as chloroform (three times) and dried under nitrogen flow to obtain **Rh^{III}(OEP)Cl**–**5**/ITO or **Rh^{III}(OEP)Cl**–**5'**/ITO, respectively.

2.1.3. *Preparation of Co^{II}(Ch)–X / ITO (X = 5, 5' or 6)*

An annealed ITO substrate was immersed in a solution of **5**, **5'**, or **6** in methanol (1.0 mM) overnight at room temperature, followed by rinsing in methanol (three times) and dried under nitrogen flow. Subsequently, the substrates were submerged in a solution of **Co^{II}(Ch)** in $CHCl_3$ (200 μM) for 3 h, followed by rinsing in $CHCl_3$ (three times) and drying in vacuo for 5 min, to obtain **Co^{II}(Ch)**–**5**/ITO, **Co^{II}(Ch)**–**5'**/ITO, or **Co^{II}(Ch)**–**6**/ITO, respectively.

2.1.4. *Preparation of Co^{II}(Ch)–X / FTO (X = 5 or 5') by Langmuir–Blodgett (LB) technique*

Fluorine doped tin oxide (FTO) coated glass slide (transmittance: 83.6%) was supplied by Sigma–Aldrich Co. LLC (US) and cut by Asahi Glass Co., Ltd. (Japan). After the **Co^{II}(Ch)** (1.2 mg) and **5** or **5'** (3.1 mg) was dissolved in $CHCl_3$ (200 μL) at room temperature, the resulted solution was air-dried in a clean hood overnight. **Co^{II}(Ch)**–**5** (4.3 mg) or **Co^{II}(Ch)**–**5'** (4.3 mg) was dissolved in $CHCl_3$ (200 μL) and sonicated for 5 min. A small portion of the $CHCl_3$ solution of **Co^{II}(Ch)**–**5** or **Co^{II}(Ch)**–**5'** (ca. 100 μL) was dropped onto the surface of purified water in the LB trough (Filgen, Japan). After evaporating $CHCl_3$ for 1.5 h, the **Co^{II}(Ch)**–**5** film or **Co^{II}(Ch)**–**5'** film were compressed by barriers at a speed of 40 mm min^{-1}. Films were deposited on glass or FTO (25 mm × 30 mm) substrates at 35 mN m^{-1} by single up-stroke withdrawal of substrate at 7 mm min^{-1}. The substrates were dried in vacuo for 5 min to remove $CHCl_3$ completely.

2.2. *Electrocatalytic hydrogen peroxide (H_2O_2) production*

Electrochemical H_2O_2 production was performed using a conventional three-electrode cell using **Co^{II}(Ch)**–**5**/FTO or **Co^{II}(Ch)**–**5'**/FTO, an Au-coil counter electrode and a Ag/AgCl reference electrode in an oxygen (O_2)–saturated aqueous perchloric acid (pH 1.3, 0.1 M, 11.0 mL) by applying constant voltage (E = 0.41 V vs. Ag/AgCl) to a working electrode. The cell was kept in dark to prevent the unexpected decomposition of produced H_2O_2. The O_2 bubbling was continued during the electrocatalytic reaction. The concentration of H_2O_2 produced in the reaction solution was determined by spectroscopic titration with an acidic solution of oxo[5,10,15,20-tetra(4-pyridyl)porphyrinato] titanium(IV) complex (Ti(TPyP)) as previously reported [26].

A similar procedure was applied for the electrochemical H_2O_2 production with **Co^{II}(Ch)**–**5**/ITO or **Co^{II}(Ch)**–**5'**/ITO in an oxygen (O_2)–saturated aqueous phthalate buffer (pH 4.01, 0.05 M) by applying constant voltage (E = –0.4 V vs. Ag/AgCl) to a working electrode to avoid corrosion of the ITO electrodes under highly acidic conditions.

3. Results and discussion

3.1. Synthesis of molecular wires

The behavior of cyclic-insulated molecules was investigated using insulated conjugated molecule **3** (Fig. 2a). Precursor **1**, bearing PM α–CD and terminal diethyl-ester-protected phosphonic acid, was prepared according to previously reported procedures [27,28]. Moreover, **1** was quantitatively converted into the corresponding insulated structure **2** by hydrophobic–hydrophilic interactions between PE and inner cavity of PM α–CD in a highly polar solvent ($MeOH/H_2O = 1/1$ (v/v)) at higher temperature (60 °C). The threading of PM α–CD was conducted on the side of the terminal nitro-group on the axis of **1**, rather than on the phosphonate group, by 360° rotation of one glucopyranose unit via the 1,4-glycosidic bonds in PM α–CD (Fig. S1) [29–32]. The quantitative conversion from **1** to **2** was confirmed from the ^1H and ^{31}P NMR spectra, wherein the protons and phosphorus in the phosphonate group shifted upfield, while the aromatic protons shifted downfield [31]. Because of the high activation barrier for the threading/dethreading transformations, heating the mixture was essential for converting **1** to **2** and vice versa. Thus, these structures displayed kinetic stability at ambient temperature. The high kinetic stability allowed the selective preparation of **3'** and **3** via deprotection of the diethyl ester groups in **1** and **2**, respectively. The ^1H NMR spectra (Fig. 2b) of **3** and **3'** confirmed successful deprotection without any unwanted changes to the insulated/uninsulated structures. In addition, insulated molecule **3** was kinetically stable, even in low-polarity solvents at room temperature for one day, in which the uninsulated structures are thermodynamically favored.

3.2. Insulation effects on the surface morphology

The insulation effects on the molecular morphologies of **3'** and **3** after their immobilization on the metal oxide surface were investigated by utilizing commercially unavailable single-crystalline ITO substrates with ultra-flat surfaces, fabricated by pulsed laser deposition on a single-crystal YSZ plate [33,34]. The single crystal ITO surface possessed regular steps derived from the single ITO layers (layer thickness, 0.3 nm) and flat terrace structures (root mean square roughness, <0.2 nm). The individual heights of **3'** and **3** on the single-crystalline ITO surfaces were easily and correctly analyzed in detail using atomic force microscopy (AFM). The crystalline ITO substrates were modified by dipping into a low-concentration (50 μM) MeOH solution of **3'** or **3**. The low concentration prevented high-density adsorption of the conjugated molecules on the ITO surface, thereby enabling the analysis of the individual height of each adsorption species by AFM. Consequently, the AFM image revealed that the single-crystalline ITO substrate was modified by the numerous protrusions of insulated conjugated molecule **3** (Fig. 2c). As shown in Figs. 2c and S6, regular step-and-terrace structures around the protrusions corresponded to the bare crystalline ITO substrate, demonstrating that the observed objects were directly and dispersively modified on the substrate without forming a molecular layer. The height distribution of this molecule on the surface mostly ranged from 0.9 to 1.9 nm (Figs. 2e and S7), which approached the calculated length of **3** (1.7 nm; Fig. S5) [35]. This indicated that the observed structure was the attached single molecule. In contrast, the formation of huge protrusions, owing to undesirable aggregation of the uninsulated conjugated molecule **3'** on the single-crystalline ITO surface, was observed (Figs. 2d, f, S8). In the histogram of immobilized **3'** (Fig. 2f, inset), the height frequently exceeded 2 nm, which was considered as aggregation, in more than 10% of the graph. This indicated that for uninsulated **3'**, surface aggregation occurred even when a low-concentration solution was utilized for surface modification. Indeed, although uninsulated **3'** possessed PM α–CD as a bulky side chain, the strong intermolecular interactions between the expanded conjugation resulted in an unfavorable aggregated structure on the ITO substrate.

3.3. Insulation effects on the interface electronic properties

To analyze the electrical properties of the immobilized molecules, **4** and **4'**, bearing redox-active ferrocene (Fc) units, were prepared (Scheme S3). NMR data supported that the PM α–CDs in **4** only covered the oligo(phenylene ethynylene) (OPE), while the Fc moiety was exposed (Figs. S3, S4). The surface coverage concentration (Γ) and other electrical properties of the **4**- or **4'**-modified ITO electrodes were then determined using cyclic voltammetry (Figs. 3a, S10, S11). The maximum Γ value of **4** was observed when the ITO substrate was immersed into a 1000 μM MeOH solution of **4** (Table S2). The Γ value of **4'** was approximately twice that of **4** (Table S3), because of the immense protrusions observed on the AFM images, which were created by aggregation of uninsulated **4'** on ITO (Fig. 3c). The plot of peak current versus scan rate (Figs. 3b, S10a) of the **4**-modified ITO electrode revealed a linear relationship, confirming that **4** was adsorbed on the electrode surface [36]. In addition, there was negligible change in the Γ value of immobilized **4** when the potential sweep was repeated 25 times (Fig. S11). This indicated that the modified surface utilizing insulated molecule **4** displayed significant redox durability.

In the cyclic voltammograms, the separation between the anodic and cathodic peaks of the redox-active species immobilized on the electrode surface is designated as 0 mV under ideal reversible conditions [36,37]. At a scan rate of 0.1 V s^{-1}, the peak-to-peak separation was 3 mV for both immobilized **4** (Fig. 3a) and immobilized **4'** (Fig. S10b). This value is small enough to be in excellent agreement with the ideal surface-adsorbed species. Moreover, the value of the full width at half maximum (FWHM) in the cyclic voltammograms was utilized to assess the immobilized molecules at the point of the electrostatic interaction with the neighboring species, as compared to the ideal width (90.6 mV at 25 °C for **4** and **4'**) [38,39]. The FWHM value of immobilized **4'** (77 mV) was smaller than the ideal value (Fig. S10b), while that of immobilized **4** (88 mV) approached the ideal value (Fig. 3a). The smaller FWHM of **4'** indicated the electrostatic attraction forces between neighboring molecules due to unwanted aggregation on the ITO surface [40]. Indeed, the redox-active Fc units were exposed for both the cases with **4** and **4'**; however, the uninsulated OPE in **4'** afforded aggregations at the interface due to the strong π-π interaction. On the other hand, the intermolecular interaction between the molecules of **4** on the ITO surface was efficiently inhibited by the [1]rotaxane structure, providing shielded π-conjugated cores at the organic–inorganic interface.

The increase in peak-to-peak separation with faster scan rates was attributed to the slow charge transfer between the ITO and immobilized redox-active species (Fc) [41,42]. The variation in the peak-to-peak separation potentials (Fig. 4a; $\Delta E = E_p - E^{\circ\prime}$, where E_p is the peak potential and $E^{\circ\prime}$ is the formal potential) with increasing scan rate was determined to construct the trumpet plots (Fig. 4b) [43–45]. While the peak-to-peak separation of uninsulated **4'** occurred at $\log(\nu) = 0.6$ ($\nu = 4$ V s^{-1}), insulated **4** did not display any significant peak-to-peak separation, even at a high scan rate of $\log(\nu) = 2$ ($\nu = 100$ V s^{-1}). This indicated that the rate of charge transfer between the ITO electrode and **4** was faster than that between the electrode and **4'**, owing to the insulated structure. The efficient interfacial charge transfer would be attributed to intramolecular charge transfer in the molecular wires, resulting from the insulation-inhibited π–π interaction between adjacent conjugated molecules on the electrode. Thus, appropriate π-aggregation inhibition at the electrode surfaces utilizing [1]rotaxanes structures is a promising strategy for developing exceptional electrical devices, owing to the high charge-transfer efficiency.

3.4. Surface functionalization with metalloporphyrin utilizing coordination bond

The molecular wires with shielded π-conjugations were then utilized to immobilize porphyrinoid complexes used as electrocatalysts. The modification of metal oxide surfaces with metalloporphyrin analogs

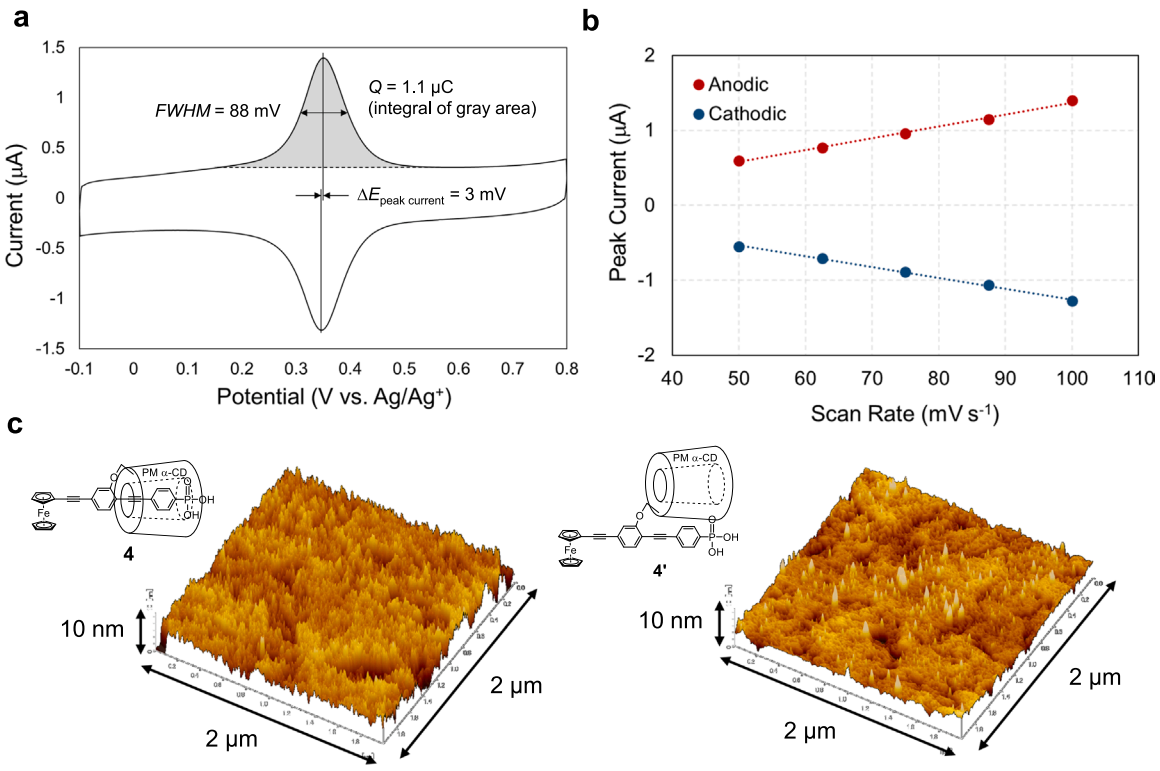

Fig. 3. (a) Cyclic voltammogram of immobilized **4** at a scan rate of 0.1 V s^{-1}. Conditions: 100 mM CH_2Cl_2 solution of tetrabutylammonium hexafluorophosphate ($TBAPF_6$). (b) Plot of anodic and cathodic peak currents of immobilized **4** versus the scan rates. (c) AFM images of the ITO substrate modified with (left) **4** and (right) **4'**.

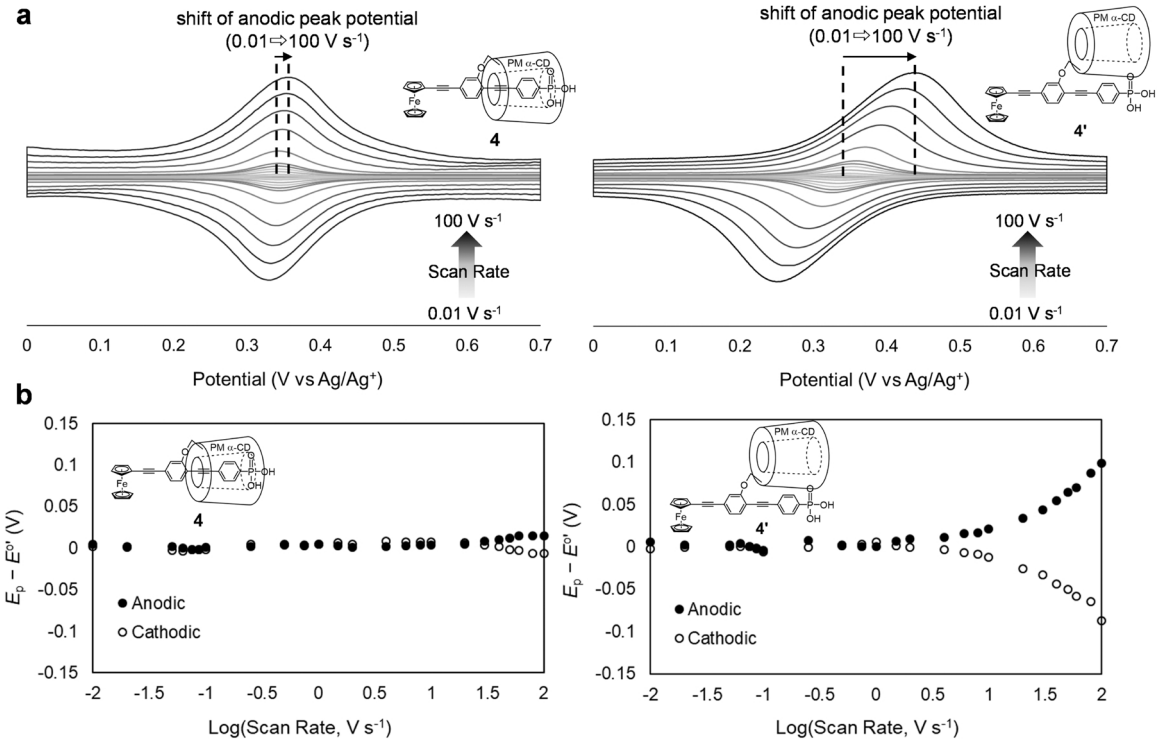

Fig. 4. (a) Cyclic voltammograms of immobilized **4** and **4'** at various scan rates. (b) Trumpet plots for immobilized **4** and **4'**. Conditions: 0.1 M CH_2Cl_2 solution of $TBAPF_6$.

have been examined in artificial photosynthesis and electrosynthesis devices [46,47]. In the current study, the 4-pyridyl group was introduced as a coordination moiety with insulated and uninsulated structures to obtain **5** and **5'**, respectively (Scheme S4). The ITO substrate was immersed in a solution of **5** or **5'** in MeOH and subsequently submerged in a solution of **Rh^{III}(OEP)Cl** (OEP: octaethylporphyrin) in

CH_2Cl_2 to obtain **Rh^{III}(OEP)Cl–5**/ITO (Fig. 5a) or **Rh^{III}(OEP)Cl–5'**/ITO, respectively. In the AFM images of the modified substrates (Fig. S17), there were no distinct aggregation structures on the surface of **Rh^{III}(OEP)Cl–5**/ITO. In contrast, many large protrusions were observed as aggregation structures on its uninsulated counterpart. Surface modification of the Rh–porphyrin complex was confirmed by UV–vis absorption and XPS analysis. In the difference UV–vis absorbance spectrum of **Rh^{III}(OEP)Cl–5**/ITO (Fig. S18b, red line), the characteristic Soret and Q bands of porphyrin were observed. Conversely, no characteristic porphyrin absorption bands were observed following the direct immersion of the ITO substrate into the **Rh^{III}(OEP)Cl** solution without immersion into a solution of **5** (Fig. S18b, blue line). Moreover, the maximum absorption wavelength of **Rh^{III}(OEP)Cl–5**/ITO corresponded to that observed in the **Rh^{III}(OEP)Cl–S12** solution (Fig. 5b). The XPS survey spectra of **Rh^{III}(OEP)Cl–5**/ITO also showed Rh 3d peaks at 310 and 315 eV (Figs. 5c, S19). These results strongly support the formation of **Rh^{III}(OEP)Cl–5** complexes with ITO as the hybrid interface. According to the integral areas of the Rh $3d_{3/2}$ and P 2p peaks, which were normalized by that of the In 3d peak derived from the ITO substrate, the Rh porphyrin-to-insulated **5** ratio in **Rh^{III}(OEP)Cl–5**/ITO was 1:1 (Table S4). On the other hand, that between Rh-porphyrin and **5'** in **Rh^{III}(OEP)Cl–5'**/ITO was 1.7:1. The mismatched equivalent ratio between **Rh^{III}(OEP)Cl** and **5'** was attributed to π-aggregation of the porphyrin complexes induced by the exposed π-conjugated molecular wires (**5'**). Thus, the modification utilizing insulated **5** allowed an easy approach for the 1:1 introduction of metalloporphyrins onto the electrode surfaces. The pyridyl group on insulated **5** allows simple electrode modification with various electrocatalytic coordination complexes via coordination bonds. In this study, modification with metalloporphyrin was achieved without complicated synthesis and aggregation on the surface. The molecular wires should act as a scaffold to allow porphyrin complexes to be carefully positioned on metal oxide surfaces with maintaining monomeric form.

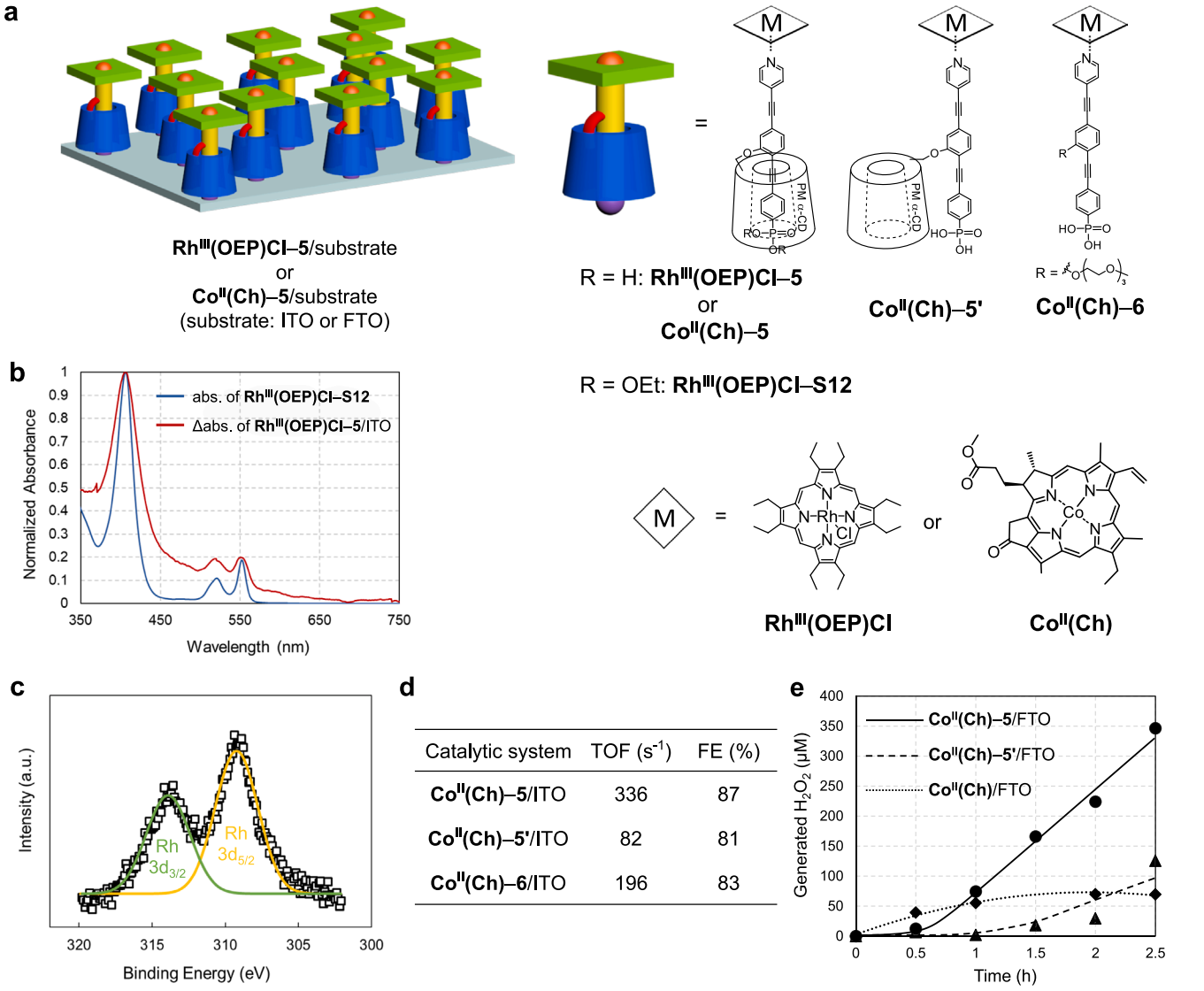

Catalytic system	TOF (s^{-1})	FE (%)
Co^{II}(Ch)–5/ITO	336	87
Co^{II}(Ch)–5'/ITO	82	81
Co^{II}(Ch)–6/ITO	196	83

Fig. 5. (a) Image of **Rh^{III}Cl(OEP)–5**/substrate and **Co^{II}(Ch)–5**/substrate. Corresponding chemical structures are shown on the right. (b) Normalized UV–vis absorption spectra of the **Rh^{III}(OEP)Cl–5**/ITO (difference spectrum of bare ITO) and $CHCl_3$ solution of the **Rh^{III}(OEP)Cl–S12** complex (1.0×10^{-5} M). Complex formation between **S12** and **Co^{II}(Ch)** in the solution state was confirmed by ^{1}H NMR and the evidence is shown in Fig. S11. (c) XPS spectra of Rh $3d_{3/2}$ (green line) and Rh $3d_{5/2}$ (yellow line) for **Rh^{III}(OEP)Cl–5**/ITO. (d) Summary of the catalytic efficiency for H_2O_2 production in **Co^{II}(Ch)–5**/ITO, **Co^{II}(Ch)–5'**/ITO, and **Co^{II}(Ch)–6**/ITO as working electrodes fabricated by stepwise modification (TOF: turnover frequency; FE: Faraday efficiency). (e) H_2O_2 production of **Co^{II}(Ch)–5**/FTO (solid line), **Co^{II}(Ch)–5'**/FTO (dashed line), and **Co^{II}(Ch)**/FTO (dotted line) fabricated by the LB method.

3.5. Electrocatalysis for H_2O_2 generation

Surface engineering using insulated molecules and metalloporphyrin derivatives was next applied to the electrical devices. The catalytic activity of **Rh^{III}(OEP)Cl-5**/ITO was examined for electrocatalytic dioxygen (O_2) reduction by CV measurements under O_2 atmosphere. However, very little catalytic current for O_2 reduction was observed during cathodic sweep from 0.5 to −1.0 V vs. Ag/AgCl (Fig. S20). Thus, **Rh^{III}(OEP)Cl** is suitable chemical species for AFM, UV-Vis and XPS measurements, however, not for catalysis examination. On the other hand, cobalt chlorin complexes (**Co^{II}(Ch)**) have been reported as highly efficient and selective molecular catalysts for the two-electron reduction of O_2 to yield hydrogen peroxide (H_2O_2) in homogeneous solution [48]. However, the selectivity decreases when **Co^{II}(Ch)** is mounted on the electrode surface with conventional methods, because disordering of mounted **Co^{II}(Ch)** results in easy formation of μ-1,2-peroxo dinuclear species which is a key intermediate of four-electron reduction of O_2 to produce H_2O [49]. In this study, the high-degree independency and outstanding electrical properties of a [1]rotaxane-based molecular wires were utilized for immobilizing **Co^{II}(Ch)** on electrode surfaces to prevent the formation of μ-1,2-peroxo dinuclear structures and enhance the charge-transfer efficiency. Insulation effects on the reaction efficiency were quantitated using the electrocatalytic system with ITO electrodes and molecular wires fabricated through stepwise modification. **Co^{II}(Ch)–5**/ITO and **Co^{II}(Ch)–5'**/ITO were formed through modification of ITO substrates with the insulated or uninsulated molecular wires (**5** or **5'**, respectively) followed by **Co^{II}(Ch)**. The adsorption amount of the **Co^{II}(Ch)** complex on the electrodes was quantified by UV–vis absorption spectroscopy (Fig. S23). During the electrocatalytic H_2O_2 synthesis, the **Co^{II}(Ch)–5**/ITO system exhibited 4-fold higher H_2O_2 production efficiency (catalytic turnover frequency (TOF), 331 s^{-1}) compared to that of the **Co^{II}(Ch)–5'**/ITO system (TOF, 82 s^{-1}; Figs. 5d, S24). The Faraday efficiency (FE) for H_2O_2 generation from O_2 in the **Co^{II}(Ch)–5**/ITO system was 87%, which was slightly higher than that of its uninsulated counterpart (**Co^{II}(Ch)–5'**/ITO system, 81%).

The number of electrons transferred to molecular O_2 was evaluated by using the rotating ring disk electrode (RRDE) system with glassy carbon and Pt electrodes as working and ring electrodes, respectively. The RRDE system uses a glassy carbon electrode, thus, quasi-dimeric molecule of **Co^{II}(Ch)–5**,(**Co^{II}(Ch)**)$_2$**–7** shown in Fig. S25a, which adsorbs on the glassy carbon substrate by **Co^{II}(Ch)** moiety instead of the phosphate linker. The limiting catalytic current for O_2 reduction increased by increasing the rotating speed from 500 to 4000 rpm as well as the Pt ring current under applied potential of 1.25 V vs. Ag/AgCl. The Levich plot based on the catalytic currents and ring currents at various rotating speeds indicated that the average number of transferred electrons was 2.47, indicating the selectivity to $2e^-$ reduction is 85%, which is similar selectivity reported in literature (Table S6).

According to the previously described experiments, π-aggregation of the uninsulated molecular wires in **Co^{II}(Ch)–5'** was detrimental to the interfacial resistance because of ineffective intermolecular charge transfer at the interface, as compared to that of its insulated counterpart. Hence, the effective intramolecular charge transfer in **Co^{II}(Ch)–5**/ITO contributes to the high TOF. In addition, the strong π–π interaction in the **Co^{II}(Ch)–5'**/ITO afforded aggregations on the ITO surface, where a part of the **Co^{II}(Ch)** molecules formed a μ-1,2-peroxo dinuclear structure, thereby leading to four-electron O_2 reduction as a side-reaction [49]. Notably, uninsulated structure (**6**), bearing a linear side chain instead of the macrocycle, also resulted in a lower H_2O_2 generation performance (TOF, 196 s^{-1}) in the catalytic system (**Co^{II}(Ch)–6**/ITO), even though the adsorbed molecular density was approximately 10 times higher than that of **Co^{II}(Ch)–5**/ITO (Fig. S23). In addition, π-aggregation on the ITO substrate of **6** was observed in the AFM experiment (Fig. S9), which deteriorated the catalytic performance of **Co^{II}(Ch)–6** due to inefficient intermolecular charge transfer, similar to what was observed with uninsulated molecular wires of **5'**. Also, UV–vis spectral measurements of **Co^{II}(Ch)–5'**/ITO at each reaction time revealed that **Co^{II}(Ch)–5'** leached from the electrode surfaces as shown in Fig. S26a, on the other hand, **Co^{II}(Ch)–5** is rather stable as shown in Fig. S26b although further stability enhancement is necessary.

The surface of substrates used for electrochemical measurements is rougher than that for AFM measurements, indicating that partially disordered alignment of **Co^{II}(Ch)–5(5')** may induce **Co^{II}(Ch)** dimer formation. Such **Co^{II}(Ch)** dimer formation is expected to result in undesired $4e^-$ reduction of O_2 to water as well as low FE. However, the FE for the reaction systems using **Co^{II}(Ch)–5**/ITO is similar to that for **Co^{II}(Ch)–5'**/ITO, indicating that only mononuclear **Co^{II}(Ch)–5'** acted as the electrocatalyst and undesired four-electron reduction of O_2 hardly proceeded. Thus, smaller turnover frequency and high FE observed for **Co^{II}(Ch)–5'**/ITO compared with those of **Co^{II}(Ch)–5**/ITO resulted from low electrocatalytic activity of dimer species probably due to inefficient electron transfer from the substrate to dimeric **Co^{II}(Ch)–5'** species, which are immobilized on the substrate in disorder or inappropriate form.

Co^{II}(Ch)–5 and **Co^{II}(Ch)–5'** were loaded onto FTO instead of ITO substrates to further evaluate the electrocatalytic H_2O_2 production, because FTO is more stable than ITO under highly acidic conditions, which are thermodynamically favorable conditions for O_2 reduction. The standard electrode potential necessary for the two-electron reduction of molecular O_2 ($O_2 + 2e^- + 2\,H^+ = H_2O_2$) is more positive under pH 1.3 than that under pH 4.01 by 0.16 V as predicted from the Nernst equation. Surface modifications of **Co^{II}(Ch)–5** and **Co^{II}(Ch)–5'** were conducted through the Langmuir–Blodgett (LB) technique under the same surface pressure, using FTO substrate to maximize the density of mononuclear **Co^{II}(Ch)** on the FTO surfaces. Both **Co^{II}(Ch)–5**/FTO and **Co^{II}(Ch)–5'**/FTO formed a solid condensed monolayer on the FTO surface, according to the pressure–area (π–A) isotherms (Fig. S27). Similar surface densities to those of **Co^{II}(Ch)–5** and **Co^{II}(Ch)–5'** on FTO were ensured by the π–A isotherms and difference absorption spectra of the modified FTO in both systems (Figs. S28, S29), and these densities were approximately four times higher than that of the abovementioned ITO system (**Co^{II}(Ch)–5**/ITO). During the electrocatalytic reaction, the **Co^{II}(Ch)–5**/FTO system showed the best H_2O_2 production efficiency (Fig. 5e). Although **Co^{II}(Ch)–5'**/FTO exhibited a similar adsorption density to that of its insulated counterpart, the performance of the **Co^{II}(Ch)–5'**/FTO system was approximately 3.5 times inferior after 2 h as compared to that of **Co^{II}(Ch)–5**/FTO. The induction periods observed for both **Co^{II}(Ch)–5**/FTO and **Co^{II}(Ch)–5'**/FTO would be due to the interaction optimization between the junction molecules and FTO substates. Such interaction optimization between junction molecules and the FTO substrate was observed owing to highly acidic conditions, where the anchor phosphate moiety of junction molecules would be partially protonated. After the induction period, the H_2O_2 concentration in the reaction solution increased linearly depending on the reaction time. Moreover, in the **Co^{II}(Ch)**/FTO system, in which the catalyst was directly deposited on the FTO surface by the LB technique, the H_2O_2 production declined after 1 h. This was attributed to catalyst desorption, owing to the lack of a phosphonic acid-based-anchoring portion in the structure. Comparison with the as-fabricated (LB technique) electrocatalytic system indicated that both the anchoring portion and insulated π-conjugation were essential to the high-performance electrocatalytic generation of H_2O_2 with the **Co^{II}(Ch)** complex. Further, high independency in the insulated structure of the junction molecules at the interface inhibited disordered aggregation. Accordingly, the [1]rotaxane structures of the junction molecules provided enhanced electrocatalytic H_2O_2 production in both systems via stepwise modification and the LB technique, improving the electron-transfer pathway and forming mononuclear complexes.

4. Conclusion

[1]Rotaxane molecules bearing a phosphonic acid-derived oligo

(phenylene ethynylene) (OPE) as the conjugated backbone and PM α–CD as a protective macrocycle were immobilized on metal oxide surfaces via a wet process. The insulated molecules were immobilized on the metal oxide surfaces in the ideal state without aggregation and displayed high charge-transfer efficiency at the interface, as compared to their uninsulated counterparts. The catalytic efficiency of the cobalt chlorin complex was markedly improved by utilizing insulated molecular wires. These results indicate the importance of the [1]rotaxane strategy in shielding molecules from unfavorable molecular interactions. The [1] rotaxane strategy can be considered as a general and versatile method for interfacial control, to upgrade the performances based on π-conjugated hybrid systems to exhibit outstanding electrocatalysis. The new strategy would provide a solution to avoid aggregation of electrocatalytic metal complexes which demand mononuclear form to exhibit their intrinsic catalytic performance.

Funding sources

This research was supported by financial supports (JSPS KAKENHI, Japan; Grant Numbers 18H05158 in Scientific Research on Innovative Areas "Innovations for LightEnergy Conversion (I4LEC)", 22H01871, 22H02060, 21K18948, 21H00018, 21K05181, and 20H02159, 19KK0144; JST CREST, Japan; Grant Number JPMJCR19I2, JST PRESTO, Japan Grant Number JPMJPR21N8, and JSPS Research Fellow, Japan). This work was performed under the Cooperative Research Program of "Network Joint Research Center for Materials and Devices".

CRediT authorship contribution statement

Yusuke Yamada: Conceptualization, Investigation, Writing – review & editing. **Jun Terao**: Conceptualization, Methodology, Writing – review & editing. **Hiroshi Masai**: Conceptualization, Investigation, Writing – original draft preparation, Writing – review & editing. **Sheng-Ying Chou**: Investigation, Writing – original draft preparation. **Gentaro Sakamoto**: Investigation. **Yusuke Kinoshita**: Investigation. **Hitoshi Tamiaki**: Investigation. **Masaya Otani**: Investigation. **Takayoshi Katase**: Investigation. **Hiromichi Ohta**: Investigation. **Tomoki Kondo**: Investigation. **Akinobu Nakada**: Investigation. **Hiromichi V. Miyagishi**: Investigation. **Ryu Abe**: Investigation. **Takahisa Tanaka**: Investigation. **Ken Uchida**: Investigation.

Declaration of Competing Interest

The authors declare that they have no known competing financial interests or personal relationships that could have appeared to influence the work reported in this paper.

Data availability

Data will be made available on request.

Acknowledgements

The authors would appreciate Kazuki Hashimoto, Shunichi Kaneko, Hiroki Hirano, and Yuichi Yasutake for their investigation for the preliminary results.

Appendix A. Supporting information

Supplementary data associated with this article can be found, in the online version, at doi:10.1016/j.apcatb.2023.122373. Materials source, instruments, synthetic procedures of junction molecules, NMR spectra of compounds, cyclic voltammograms of modified surfaces, AFM analyses of modified surfaces, methods of computational calculations and the optimized structures, titration results, UV–vis absorption spectra, XPS spectra, and pressure-area isotherms (PDF).

References

[1] Y.W. Muhammed, Recent advances in energy storage systems for renewable source grid integration: a comprehensive review, Sustainability 14 (2022) 5985, https://doi.org/10.3390/su14105985.
[2] S. Berardi, S. Drouet, L. Francàs, C. Gimbert-Suriñach, M. Guttentag, C. Richmond, T. Stoll, A. Llobet, Molecular artificial photosynthesis, Chem. Soc. Rev. 43 (2014) 7501–7519, https://doi.org/10.1039/C3CS60405E.
[3] Y. Wen, T. Zhang, J. Wang, Z. Pan, T. Wang, H. Yamashita, X. Qian, Y. Zhao, Electrochemical reactors for continuous decentralized H_2O_2 production, Angew. Chem. Int. Ed. 61 (2022), https://doi.org/10.1002/anie.202205972.
[4] X. Chen, Y. Kondo, Y. Kuwahara, K. Mori, C. Louis, H. Yamashita, Metal-organic framework-based nanomaterials for photocatalytic hydrogen peroxide production, Phys. Chem. Chem. Phys. 22 (2020) 14404–14414, https://doi.org/10.1039/D0CP01759K.
[5] Y. Shiraishi, M. Matsumoto, S. Ichikawa, S. Tanaka, T. Hirai, Polythiophene-doped resorcinol–formaldehyde resin photocatalysts for solar-to-hydrogen peroxide energy conversion, J. Am. Chem. Soc. 143 (2021) 12590–12599, https://doi.org/10.1021/jacs.1c04622.
[6] Y. Yamada, Y. Fukunishi, S. Yamazaki, S. Fukuzumi, Hydrogen peroxide as sustainable fuel: electrocatalysts for production with a solar cell and decomposition with a fuel cell, Chem. Commun. 46 (2010) 7334–7336, https://doi.org/10.1039/c0cc01797c.
[7] R.A. Durst, A.J. Baumner, R.W. Murray, R.P. Buck, C.P. Anderieux, Chemically modified electrodes: recommended terminology and definitions, Pure Appl. Chem. 69 (1997) 1317–1323, https://doi.org/10.1351/pac199769061317.
[8] H. Iwami, M. Okamura, M. Kondo, S. Masaoka, Electrochemical polymerization provides a function-integrated system for water oxidation, Angew. Chem. Int. Ed. 60 (2021) 5965–5969, https://doi.org/10.1002/anie.202015174.
[9] Z.N. Zahran, Y. Tsubonouchi, E.A. Mohamed, M. Yagi, Recent advances in the development of molecular catalyst-based anodes for water oxidation toward artificial photosynthesis, ChemSusChem 12 (2019) 1775–1793, https://doi.org/10.1002/cssc.201802795.
[10] A. Vilan, D. Cahen, Chemical modification of semiconductor surfaces for molecular electronics, Chem. Rev. 117 (2017) 4624–4666, https://doi.org/10.1021/acs.chemrev.6b00746.
[11] P.J. Hotchkiss, S.C. Jones, S.A. Paniagua, A. Sharma, B. Kippelen, N.R. Armstrong, S.R. Marder, The modification of indium tin oxide with phosphonic acids: mechanism of binding, tuning of surface properties, and potential for use in organic electronic applications, Acc. Chem. Res. 45 (2012) 337–346, https://doi.org/10.1021/ar200119g.
[12] Y. Huang, E.J. Kramer, A.J. Heeger, G.C. Bazan, Bulk heterojunction solar cells: morphology and performance relationships, Chem. Rev. 114 (2014) 7006–7043, https://doi.org/10.1021/cr400353v.
[13] L. Zhang, J.M. Cole, Dye aggregation in dye-sensitized solar cells, J. Mater. Chem. A 5 (2017) 19541–19559, https://doi.org/10.1039/C7TA05632J.
[14] F. Cacialli, J.S. Wilson, J.J. Michels, C. Daniel, C. Silva, R.H. Friend, N. Severin, P. Samorì, J.P. Rabe, M.J. O'Connell, et al., Cyclodextrin-threaded conjugated polyrotaxanes as insulated molecular wires with reduced interstrand interactions, Nat. Mater. 1 (2002) 160–164, https://doi.org/10.1038/nmat750.
[15] M.J. Frampton, H.L. Anderson, Insulated molecular wires, Angew. Chem. Int. Ed. 46 (2007) 1028–1064, https://doi.org/10.1002/anie.200601780.
[16] H. Masai, Y. Oka, J. Terao, Precision synthesis of linear oligorotaxanes and polyrotaxanes achieving well-defined positions and numbers of cyclic components on the axle, Chem. Commun. 48 (2022) 1644–1660, https://doi.org/10.1039/d1cc03507j.
[17] J.C. Wang, S.P. Hill, T. Dilbeck, O.O. Ogunsolu, T. Banerjee, K. Hanson, Multimolecular assemblies on high surface area metal oxides and their role in interfacial energy and electron transfer, Chem. Soc. Rev. 47 (2018) 104–148, https://doi.org/10.1039/c7cs00565b.
[18] M. Freitag, E. Galoppini, Molecular host-guest complexes: shielding of guests on semiconductor surfaces, Energy Environ. Sci. 4 (2011) 2482–2494, https://doi.org/10.1039/c0ee00396d.
[19] C. Pagba, G. Zordan, E. Galoppini, E.L. Piatnitski, S. Hore, K. Deshayes, P. J. Piotrowiak, Hybrid photoactive assemblies: electron injection from host−guest complexes into semiconductor nanoparticles, J. Am. Chem. Soc. 126 (2004) 9888–9889, https://doi.org/10.1021/ja0475252.
[20] Y. Domi, K. Ikeura, K. Okamura, K. Shimazu, M.D. Porter, Strong inclusion of inorganic anions into β-cyclodextrin immobilized to gold electrode, Langmuir 27 (2011) 10580–10586, https://doi.org/10.1021/la1051063.
[21] M. Xue, Y. Yang, X. Chi, X. Yan, F. Huang, Development of pseudorotaxanes and rotaxanes: from synthesis to stimuli-responsive motions to applications, Chem. Rev. 115 (2015) 7398–7501, https://doi.org/10.1021/cr5005869.
[22] A. Leventis, J. Royakkers, A.G. Rapidis, N. Goodeal, M.K. Corpinot, J.M. Frost, D. K. Bučar, M.O. Blunt, F. Cacialli, H. Bronstein, Highly luminescent encapsulated narrow bandgap polymers based on diketopyrrolopyrrole, J. Am. Chem. Soc. 140 (2018) 1622–1626, https://doi.org/10.1021/jacs.7b13447.
[23] C. Pan, C. Zhao, M. Takeuchi, K. Sugiyasu, Conjugated oligomers and polymers sheathed with designer side chains, Chem. –Asian J. 10 (2015) 1820–1835, https://doi.org/10.1002/asia.201500452.
[24] C. Queffélec, M. Petit, P. Janvier, D.A. Knight, B. Bujoli, Surface modification using phosphonic acids and esters, Chem. Rev. 112 (2012) 3777–3807, https://doi.org/10.1021/cr2004212.
[25] R. Yasuhara, S. Murai, K. Fujita, K. Tanaka, Atomically smooth and single crystalline indium tin oxide thin film with low optical loss, Phys. Status Solidi Curr.

Top. Solid State Phys. 9 (2012) 2533–2536, https://doi.org/10.1002/pssc.201200303.
[26] C. Matsubara, N. Kawamoto, K. Takamura, Oxo[5, 10, 15, 20-tetra(4-pyridyl)porphyrinato]titanium(IV): an ultra-high sensitivity spectrophotometric reagent for hydrogen peroxide, Analyst 117 (1992) 1781–1784, https://doi.org/10.1039/AN9921701781.
[27] M. Kalek, M. Jezowska, J. Stawinski, Preparation of Arylphosphonates by Palladium(O)-Catalyzed Cross-Coupling in the Presence of Acetate Additives: Synthetic and Mechanistic Studies, Adv. Synth. Catal. 351 (2009) 3207–3216, https://doi.org/10.1002/adsc.200900590.
[28] H. Masai, J. Terao, T. Fujihara, Y. Tsuji, Rational design for rotaxane synthesis through intramolecular slippage: control of activation energy by rigid axle length, Chem. Eur. J. 22 (2016) 6624–6630, https://doi.org/10.1002/chem.201600429.
[29] Motion of threading/dethreading transformation is shown in Figure S1 in the supporting information.
[30] S.Y. Chou, H. Masai, S. Tsuda, J. Terao, Synthetic methodology for structurally defined and insulated molecular wires bearing non-centrosymmetric conjugated axle components via iterative intramolecular slippage, Chem. Asian J. 14 (2019) 1667–1671, https://doi.org/10.1002/asia.201801706.
[31] H. Masai, J. Terao, Synthetic methodologies for structurally defined linked-[n] rotaxanes with permethylated cyclodextrins: platform for functionalized molecular electronics, Bull. Chem. Soc. Jpn 92 (2019) 529–539, https://doi.org/10.1246/bcsj.20180349.
[32] R. Nishiyabu, K. Kano, Double self-inclusion by rotating glucopyranose units in per-o-methylated β-cyclodextrin moieties attached to a porphyrin in aqueous solution, Eur. J. Org. Chem. 24 (2004) 4985–4988, https://doi.org/10.1002/ejoc.200400309.
[33] H. Ohta, M. Orita, M. Hirano, H. Hosono, Surface morphology and crystal quality of low resistive indium tin oxide grown on yittria-stabilized zirconia, J. Appl. Phys. 91 (2002) 3547–3550, https://doi.org/10.1063/1.1448873.
[34] H. Ohta, T. Kambayashi, M. Hirano, H. Hoshi, K. Ishikawa, H. Takezoe, H. Hosono, Application of transparent conductive substrate with atomically flat & stepped surface for lateral growth of organic molecule: vanadyl-phthalocyanine, Adv. Mater. 15 (2003) 1258–1262, https://doi.org/10.1002/adma.200345041.
[35] (a) AFM would underestimate the absolute height of 3 immobilized on the surface of a single-crystalline ITO because of the softness of 3 and the interaction between the AFM probe and sample surface according to the following references Y. Jiao, T. E. Schäffer, Accurate Height and Volume Measurements on Soft Samples with the Atomic Force Microscope, Langmuir 20 (2004) 10038–10045, https://doi.org/10.1021/la048650u;
(b) Y. Ebenstein, E. Nahum, U. Banin, Tapping Mode Atomic Force Microscopy for Nanoparticle Sizing: Tip-Sample Interaction Effects, Nano Lett. 2 (2002) 945–950, https://doi.org/10.1021/nl025673p.
[36] A.L. Eckermann, D.J. Feld, J.A. Shaw, T.J. Meade, Electrochemistry of redox-active self-assembled monolayers, Coord. Chem. Rev. 254 (2010) 1769–1802, https://doi.org/10.1016/j.ccr.2009.12.023.
[37] N. Elgrishi, K.J. Rountree, B.D. McCarthy, E.S. Rountree, T.T. Eisenhart, J. L. Dempsey, A practical beginner's guide to cyclic voltammetry, J. Chem. Educ. 95 (2018) 197–206, https://doi.org/10.1021/acs.jchemed.7b00361.
[38] A.J. Bard, R.L. Faulkner, Electrochemical Methods: Fundamentals and Applications, 2nd ed..,, John Wiley&Sons, Inc,, New York, 2001.
[39] L.Y.S. Lee, T.C. Sutherland, S. Rucareanu, R.B. Lennox, Ferrocenylalkylthiolates as a Probe of Heterogeneity in Binary Self-Assembled Monolayers on Gold, Langmuir 22 (2006) 4438–4444, https://doi.org/10.1021/la053317r.
[40] H. Tian, Y. Dai, H. Shao, H.Z. Yu, Modulated intermolecular interactions in ferrocenylalkanethiolate self-assembled monolayers on gold, J. Phys. Chem. C. 117 (2013) 1006–1012, https://doi.org/10.1021/jp310012v.
[41] L.H. Guo, J.S. Facci, G. McLendon, Distance dependence of electron transfer rates in bilayers of a ferrocene langmuir-blodgett monolayer and a self-assembled monolayer on gold, J. Phys. Chem. 99 (1995) 8458–8461, https://doi.org/10.1021/j100021a002.
[42] Y. Guo, J. Zhao, J. Zhu, Study on the Intermolecular Interactions between the Functional Moieties in Ferrocene-Terminated Alkanethiol Self-Assembled Monolayer on Gold, Thin Solid Films 516 (2008) 3051–3057, https://doi.org/10.1016/j.tsf.2007.12.092.
[43] T. Steentjes, P. Jonkheijm, J. Huskens, Electron transfer processes in ferrocene-modified poly(ethylene glycol) monolayers on electrodes, Langmuir 33 (2017) 11878–11883, https://doi.org/10.1021/acs.langmuir.7b02160.
[44] C.M. Hanna, C.D. Sanborn, S. Ardo, J.Y. Yang, Interfacial electron transfer of ferrocene immobilized onto indium tin oxide through covalent and noncovalent interactions, ACS Appl. Mater. Interfaces 10 (2018) 13211–13217, https://doi.org/10.1021/acsami.8b01219.
[45] L. Wang, D.E. Polyansky, J.J. Concepcion, Self-assembled bilayers as an anchoring strategy: catalysts, chromophores, and chromophore-catalyst assemblies, J. Am. Chem. Soc. 141 (2020) 8020–8027, https://doi.org/10.1021/jacs.9b01044.
[46] N. Han, Y. Wang, L. Ma, J. Wen, J. Li, H. Zheng, K. Nie, X. Wang, F. Zhao, Y. Li, J. Fan, J. Zhong, T. Wu, D.J. Miller, J. Lu, S.T. Lee, Y. Li, Supported Cobalt Polyphthalocyanine for High-Performance Electrocatalytic CO_2 Reduction, Chem 3 (3) (2017) 652–664, https://doi.org/10.1016/j.chempr.2017.08.002.
[47] K.E. Dalle, J. Warnan, J.J. Leung, B. Reuillard, I.S. Karmel, E. Reisner, Electro- and solar-driven fuel synthesis with first row transition metal complexes, Chem. Rev. 119 (2019) 2752–2875, https://doi.org/10.1021/acs.chemrev.8b00392.
[48] K. Mase, K. Ohkubo, S. Fukuzumi, Efficient two-electron reduction of dioxygen to hydrogen peroxide with one-electron reductants with a small overpotential catalyzed by a cobalt chlorin complex, J. Am. Chem. Soc. 135 (2013) 2800–2808, https://doi.org/10.1021/ja312199h.
[49] K. Mase, M. Yoneda, Y. Yamada, S. Fukuzumi, Seawater usable for production and consumption of hydrogen peroxide as a solar fuel, Nat. Commun. 7 (2016) 11470, https://doi.org/10.1038/ncomms11470.